GENESIS PHASE A/B1

Tools for GENESIS scientific data exploitation

GENESIS VLBI Transmitter

ROB/AWS/UCLouvain/ULiège (Belgium)

	Signature
Written by	**AUTHORS**
H. Sert, V. Dehant (ROB)	
Verified by	**CHECKERS**
Approved	**APPROVERS**
Responsibilities	**RESPONSIBILITIES OF THE ABOVE-MENTIONED PERSONS**
O. Karatekin (ROB)	**Principal Investigator**
B. Ritter (ROB)	**Co-Principal Investigator**

CHANGE RECORDS

ISSUE V.x.y[1]	DATE (dd/mm/year)	CHANGE RECORDS	Reason for change
V1.1(1) draft	14/01/2025	New document	Following H. Sert's report for PRODEX
V1.1(2)	xx/xx/2025	xxxx	xxxx

[1] Vx.y ==> x = version number, y = issue number

TABLE OF CONTENTS

1. GENERAL INFORMATION

1.1 Scope of the Document

The document aims to detail the development of software and the simulations for GENESIS mission.

1.2 Applicable documents

Title	*Reference*
GENESIS-ROB-AA-0001-Abbreviations-Acronyms_v1.1 provides the abbreviations and acronyms used in this context.	GENESIS-ROB-AA-0001

1.3 Reference documents

Title	*Reference*
Technical Note for Precise Orbit Determination (POD) for GENESIS	GENESIS-ROB-TN-0001
Technical Note on GENESIS data product providing documentation on what GENESIS can bring for science and society	GENESIS-ROB-TN-0002

2. VISIBILITY ANALYSIS OF GENESIS

To assess the visibility of GENESIS by VGOS stations, we generated an orbit with an altitude of 6000km and an inclination of 95º. Figure 1 illustrates the ground track of GENESIS satellite for one day, along with the VGOS network selected for the simulations. The period of a circular polar orbit at 6000km is around 4 hours. Figure 2 shows the elevation angles of GENESIS satellite in the sky of each VGOS station and it can be seen that maximum elevation is repeated approximatively every 4 hours.

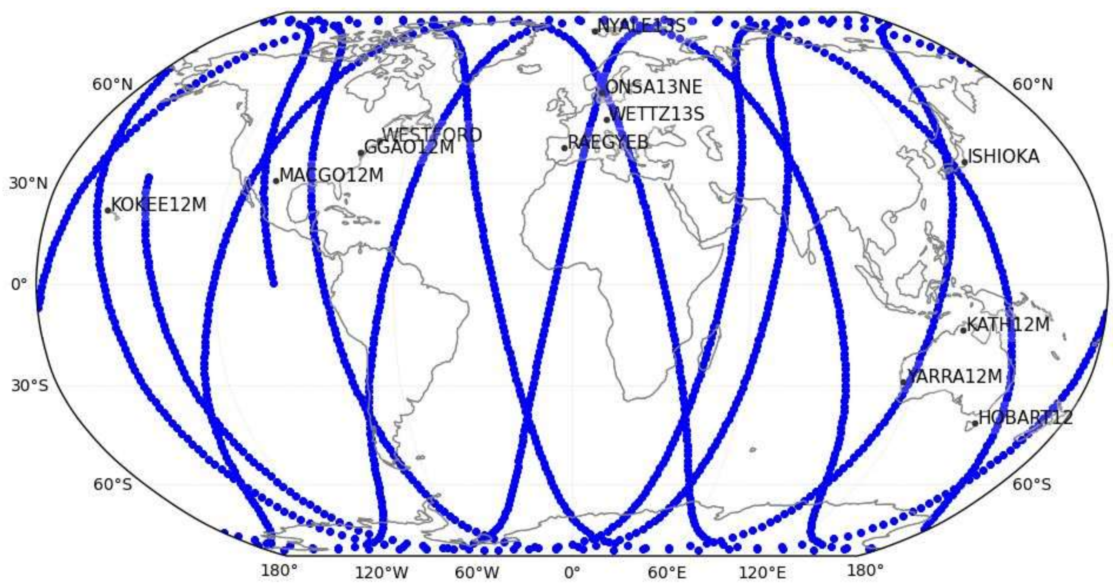

Figure 1. Ground track of GENESIS for one day and VGOS stations

To further elaborate on the station visibilities, we show the observation windows and their durations of GENESIS observation at each station in the VGOS network in Figure 3. It should be noted that the number of visibility windows may vary depending on the initial geometrical configuration between the satellite and the Earth. Nevertheless, the figure provides a clear representation of the visibility opportunities.

While the visibility of individual stations is important, VLBI observations require simultaneous visibility from at least two stations to achieve a common baseline. Observations from a single station are insufficient for traditional VLBI techniques. Figure 4 shows the average baseline visibility durations for each baseline within the network.

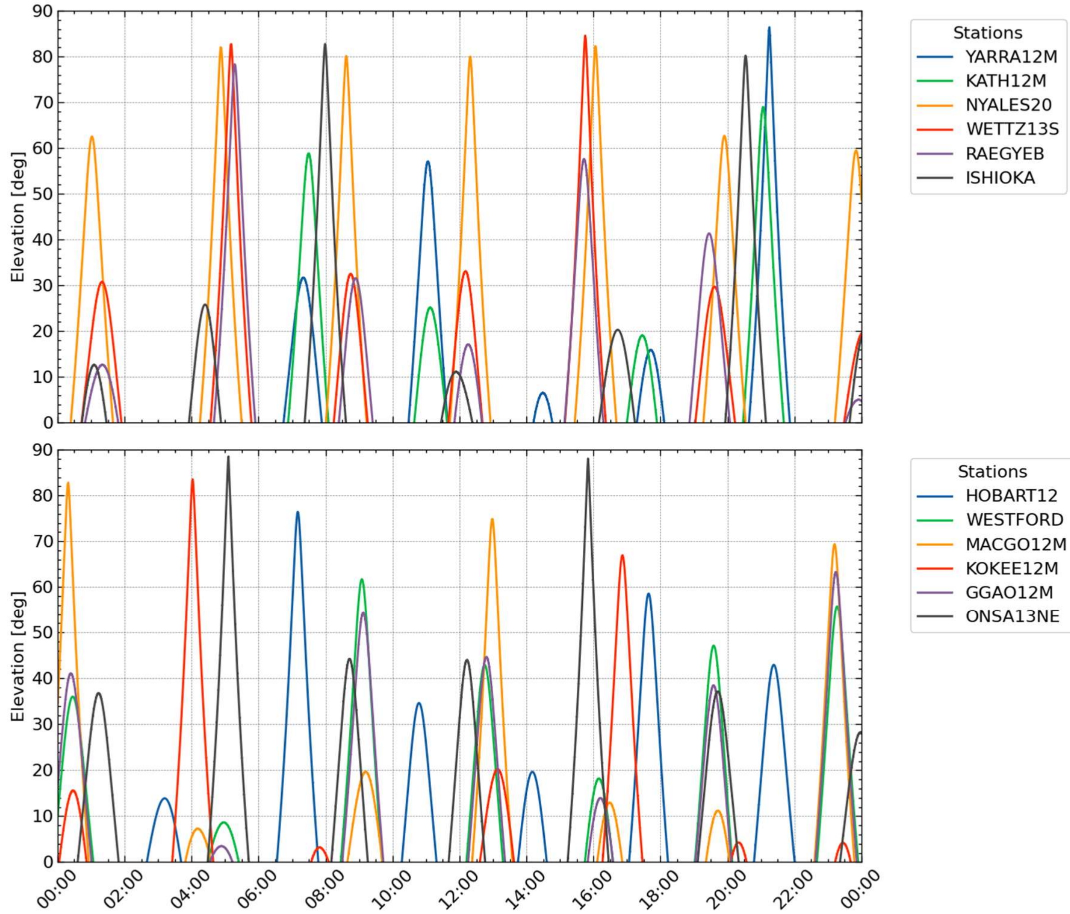

Figure 2: Elevation of GENESIS for the VGOS stations.

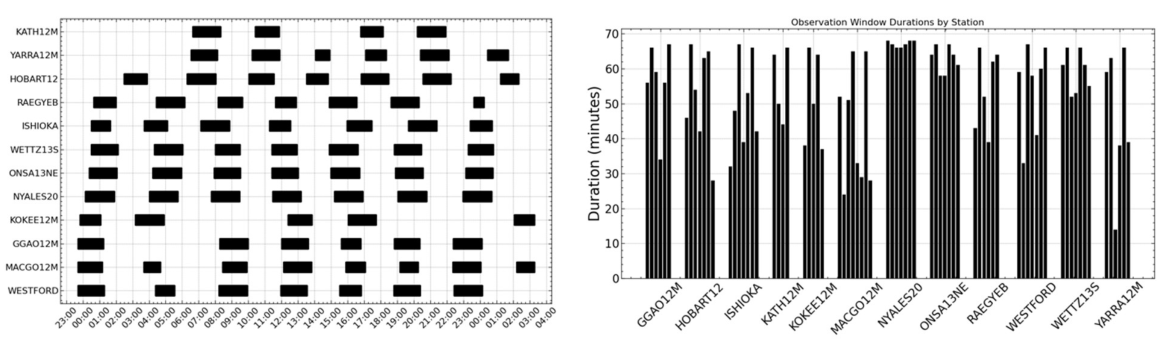

Figure 3: Observability windows of GENESIS for the VGOS stations.

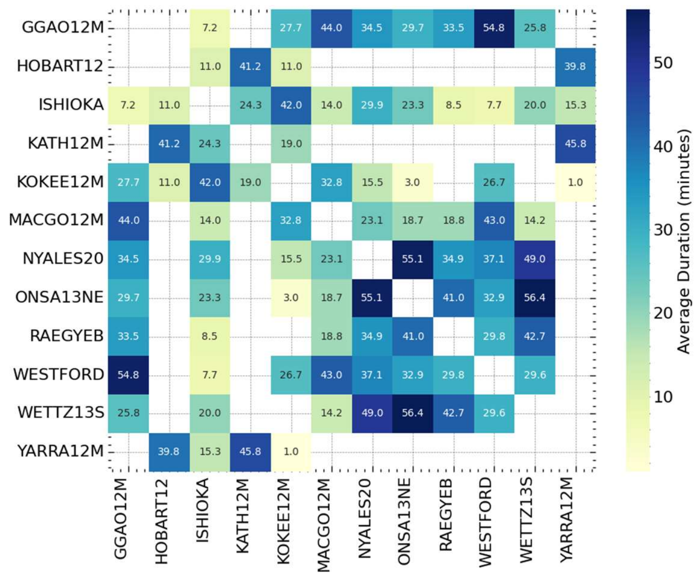

Figure 4. Average baseline visibility durations of VGOS network.

3. DATA ANALYSIS SOFTWARE

Observation of an Earth orbiting VT source by VLBI ground stations requires a delay model in which the curvature of the wavefront is taken into account. The concept of VT observations is illustrated in Figure 1 where the satellite emits a signal at t_0, which then reaches the two stations at $t_1$and t_2 respectively. The time delay between the arrival times at the two ground stations is given as

$$\tau = t_2 - t_1.$$

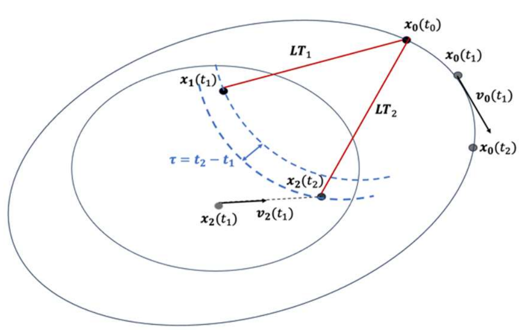

Figure 1. Concept of emission and transmission times for VLBI observation of a satellite.

Several near-field models have been proposed in the literature to determine the time delay between stations. We compared the most commonly used models, along with an additional model that analytically solves the light-time equation. Table 1 summarizes the models used in our study and their main approaches.

Table 1: Near-field VLBI delay models used in the study.

Model	Approach
Klioner (1991)	Taylor expansion for t_0
Fukushima (1994)	Introducing pseudo source vector $\vec{K}$
Duev (2012)	Iterative solutions for t_0 and t_2
Jaron & Nothnagel (2019)	Analytical solutions for t_0 and t_2

As a first step, we simulate a simple geometrical configuration in which a VT source is positioned at the zenith of the first station, located at the equator on the prime meridian. The second station is also positioned on the equator but at a longitude of 20 degrees. Delays are computed using four different near-field models for a VT source at varying altitudes. Figure 2 compares these models across different altitudes for this basic geometrical setup. As observed in the figure, all models (except Klioner's) show consistency within 10^{-18}seconds for altitudes below 6000 km. Klioner's model, while slightly deviating, still achieves consistency within 10^{-14} seconds, which is two orders of magnitude better than the precision threshold of 1 picosecond (10^{-12} seconds). At higher altitude, the divergence between the models increases but it remains below 1 picosecond for altitude under 10^8 km.

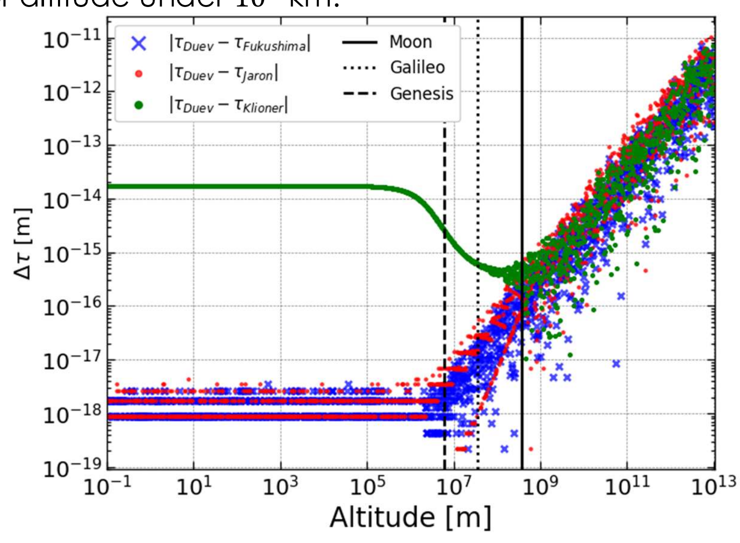

Figure 2. Vacuum delay differences for simple test cases where the first station is located at longitude $\lambda = 0^o$, and latitude $\delta = 0^o$. Second station is located at $\lambda = 20^o$and $\delta = 0^o$. VT source is located at the zenith of the first station with various altitudes.

The results in Figure 2 are based on simple geometrical configuration and the satellite position is (back) propagated using the following kinematical equation which linearizes the trajectory:

$$x_0(t_0) = x_0(t_1) + v_0(t_1)(t_0 - t_1)$$

To make a more realistic analysis, we use the VGOS network given in Figure 3 and we propagate the orbit using numerical integration. The orbit is chosen to be at 6000 km altitude with an inclination of 95^o degrees, which represents the orbital configuration of GENESIS.

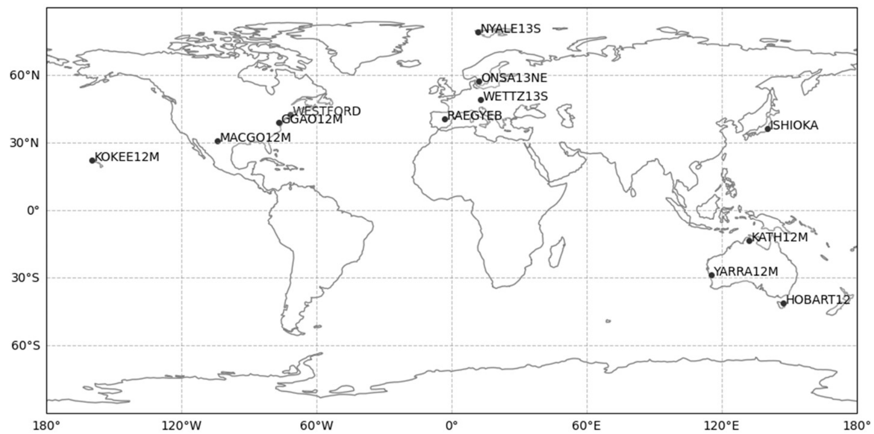

Figure 3. Network of VGOS station for the simulations.

Figure 4 illustrates the delay differences for the GENESIS satellite over the course of a day, comparing various near-field models against Duev's model. The figure highlights that when satellite orbits are numerically propagated in the iterative solution of the light-time equation to determine the satellite emission time, the analytical model by Jaron & Nothnagel diverges from Duev's model by an order of magnitude at the picosecond. In contrast, the other models exhibit error levels consistent with those observed in the simple geometrical configuration shown in Figure 2. This divergence observed with Jaron & Nothnagel's model is likely due to their reliance on an analytical model's approach, which does not solve the light-time equation directly but instead assumes a linearized satellite trajectory to calculate the emission time, $\mathbf{t_0}$.

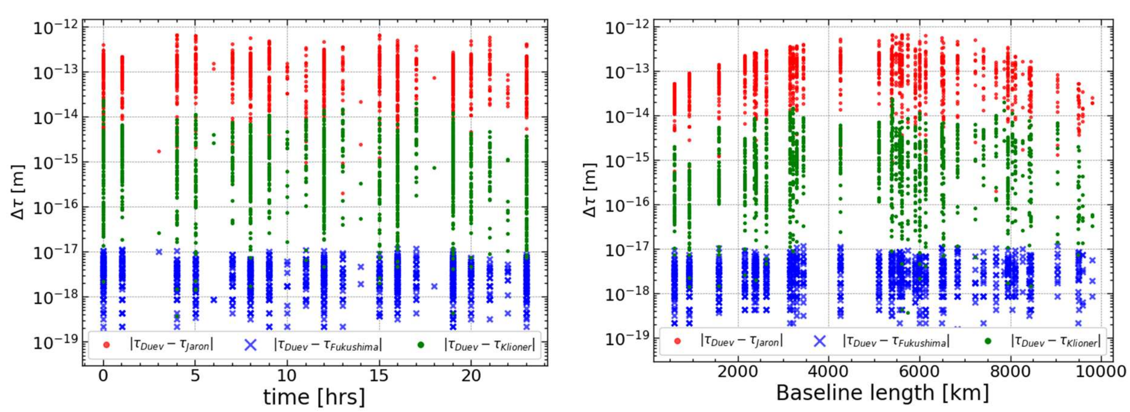

Figure 4. Comparison of near-field delay models over time (Left) and as a function of baseline length (Right) for the VLBI network.

To provide a clearer understanding of the effect of the geometrical configuration between the source and the stations on the delay differences computed from two different near-field models, we analyze the influence of the elevation angles of the satellite ($\boldsymbol{\varepsilon}$) at two different stations ($\boldsymbol{\varepsilon_1}, \boldsymbol{\varepsilon_2}$) on the corresponding delay differences computed against Duev's model (Dt) for Fukushima's, Klioner's, and Jaron & Nothnagel's near-field models. Figure 5 illustrates the impact of the geometrical configuration for those different pairs of models. As shown in the figure, no significant geometrical sensitivity is observed between the Duev and Fukushima models, which is expected as both determine the signal emission time ($\mathbf{t_0}$) by solving the light-time equation. However, the delay differences from Klioner's and Jaron & Nothnagel's models against Duev's model exhibit a noticeable "diagonal" geometrical sensitivity. When the elevation angles at both stations in the baseline are similar, the differences between the models appear to be consistent and aligned.

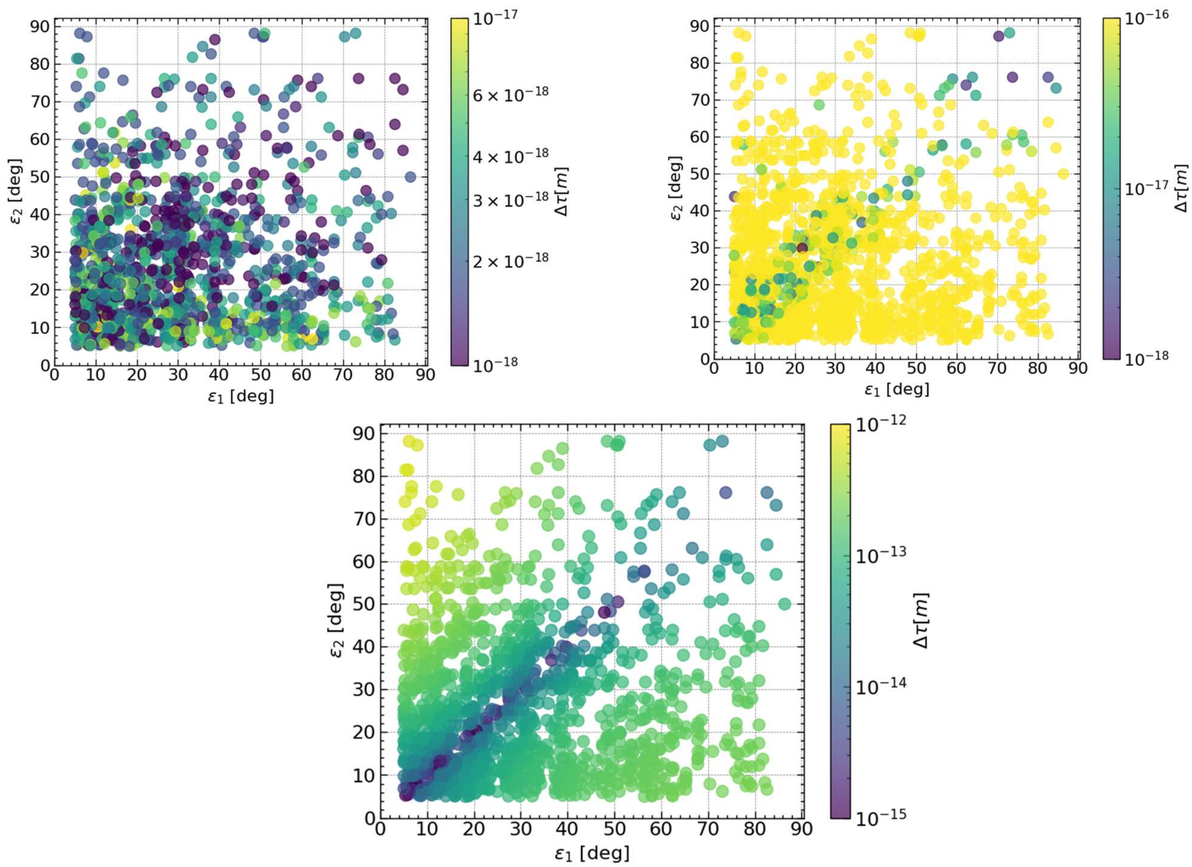

Figure 5. Comparison of near-field models during a day $|\tau_{Duev} - \tau_{Fukushima}|$ (Left), $|\tau_{Duev} - \tau_{Klioner}|$ (Middle), and $|\tau_{Duev} - \tau_{Jaron}|$ (Right).

4. USAGE OF GEODETIC ANALYSIS SOFTWARE C5++

C5++ is a geodetic analysis software evolved from the CONCERTO4 package developed by Otsubo et al. (1994). Originally implemented in Java, CONCERTO4 was designed to process satellite-based techniques such as SLR and GPS. With the need for software updates and a shift away from Java, the new version was rewritten and redesigned in C++, renamed as C5++, and also includes a VLBI module to process quasar observations. C5++ is developed among three Japanese research groups which are located at Hitotsubashi University, NICT and JAXA.

In C5++, all observation techniques are represented as class objects with a specific naming convention: “Player+Techniquename” (e.g., “PlayerVlbi”, “PlayerSlr”, ...). Each “Player” represents a space geodetic. For each Player the most important common methods of all players are “Init” and “Play” commands. The Init run command is executed once for each observation technique to initialize parameters, input files, a priori information, models and other setup requirements. All observations from each technique are then submitted into a common pool, along with their associated errors, to be processed iteratively together. Following initialization, the “Play” run command processes all observations for all different techniques iteratively. This involves computing the observed-computed (O-C) values, observation errors, and partial derivatives, which are used to update the system of equations involving all the parameters that are determined. After all observations have been processed, the normal equation (NEQ) system is solved, and the parameters are updated. Next, the weighted root mean square (WRMS) errors are calculated, and variance scale factors for individual observation series are updated. The Play run is then executed again with updated parameters as well as newly determined variance factors. This process repeats until the WRMS of NEQ system converges. Once the iteration process is complete, the estimated parameters are written in a (extended-)SINEX file as output.

The ROB team has extensively studied C5++ and the software is understood. Figure 6 shows the flow chart of the software to carry out an estimation procedure. To test the software, SLR, and GNSS observations have been processed to estimate station coordinate positions. Additionally, focusing VLBI quasar observations, we estimate UT1-UTC observations using intensive VLBI sessions for the year 2017. Both legacy and VGOS types of observation data are processed. Figure 7 shows the formal errors of UT1-UTC obtained by both observation types.

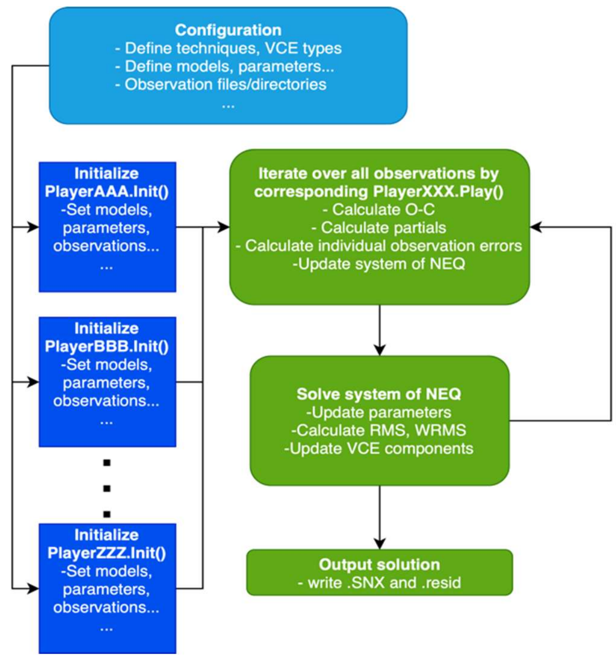

Figure 6. Flow chart of C5++.

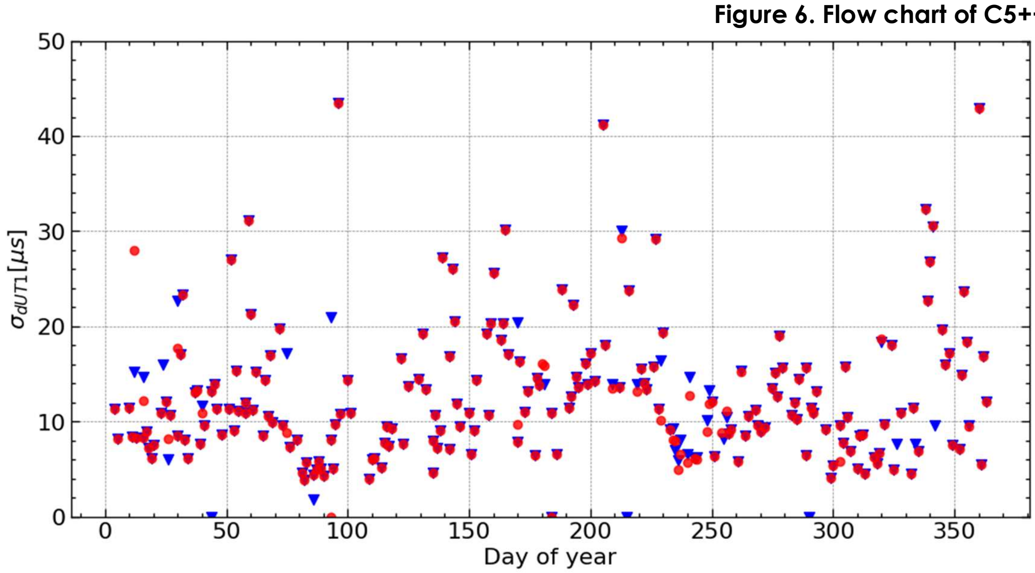

Figure 7. Formal precision of UT1-UTC observations for a year. (Red) from legacy VLBI observations and (Blue) from VGOS observations.

5. IMPLEMENTATION OF VT SIMULATIONS INTO C5++

After being able to use the software, a new player, PlayerVTSIM is implemented into the software. PlayerVTSIM is a player which first simulates VLBI Transmitter observations onboard a satellite for given parameters then runs an estimation procedure using the simulated observations. Figure 8 summarizes the flow chart of the new player.

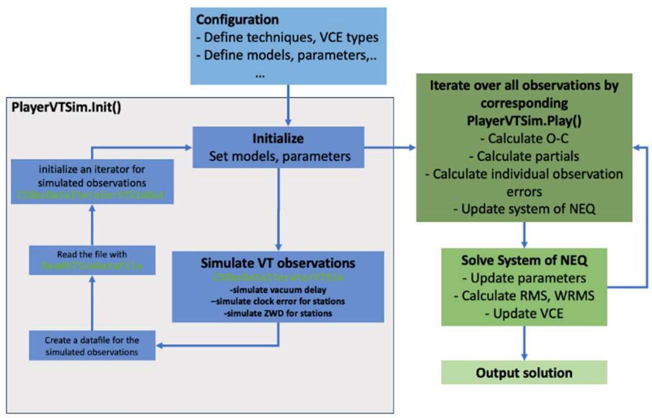

Figure 8. Flow chart of PlayerVTSIM.

In the PlayerVTSIM, all four near-field VLBI observation models are implemented. Users can pick one of them in the configuration file. In order to simulate realistic VT observations, one needs to consider the effect of the wet part of the troposphere and station clock errors, as these need to be estimated without a priori model in hand. An observation residual can be represented by:

$$\mathbf{O - C = (zwd_2\ mfw_2(e) + clock_2) - (zwd_1\ mfw_1(e) + clock_1) + wn}$$

where $\mathbf{zwd_i}$, $\mathbf{mfw_i}$, and $\mathbf{clock_i}$ represent equivalent zenith wet delay (EZWD), mapping function (function of the elevation e) and clock error for station $\mathbf{i}$. $\mathbf{wn}$ represents the white noise for a VLBI observation which is typically 4 picoseconds for VGOS stations. Simulators for EZWD and station have been implemented in the software and can be activated in the configuration file for various parameters.

Figure 9 shows simulated EZWD errors at different elevation angles and for different stations during one day. The adjustable parameters to simulate EZWD for VT observations are structure constant (quantifying the intensity of atmospheric turbulence in terms of refractivity fluctuations), saturation length scale (referring to the upper limit on the size of turbulent eddies in the atmosphere and representing the largest scale at which turbulent energy is injected into the atmosphere), and a priori error on the horizontal/vertical wind speeds. Each of them can be parameterized in the configuration file. To simulate station clock errors, random and integrated random walks are used for given Allan deviation values. Figure 10 shows the simulated clock errors for 4 stations during a day. As can be seen in the Figures below, elevation dependency and stochastic behavior of the EZWD are as expected for given a priori error of 10 centimeters. Additionally, station clock behavior follows also realistic behavior which was also cross-checked with commonly used VLBI processing software VieVs (Vienna VLBI Software). For each VT simulations, at each observation epoch EZWD and station clock errors can now be included in C5++ software.

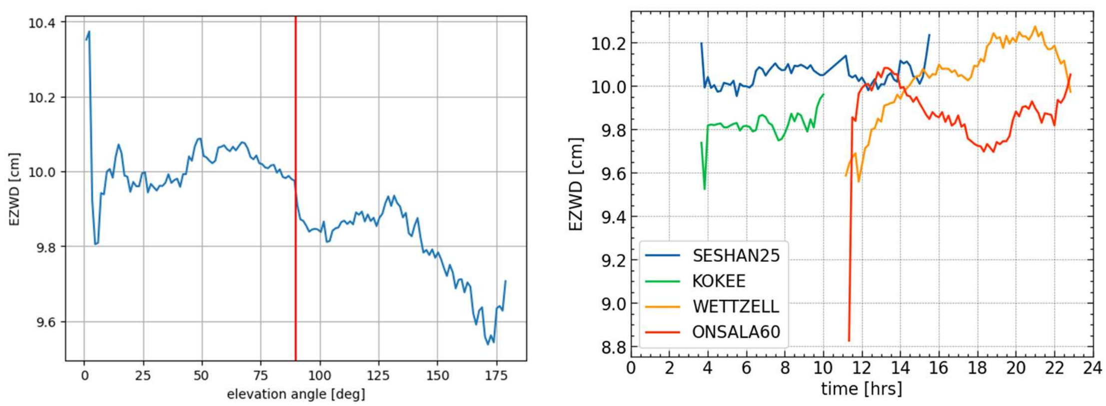

Figure 9. Equivalent zenith wet delay error simulations. (Left) elevation dependency (Right) For different stations during one-day.

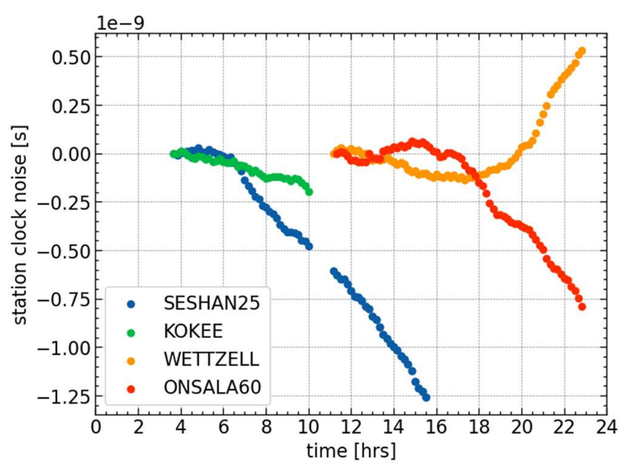

Figure 10. Simulated station clock errors for different stations.

Link budget calculations of VT onboard GENESIS satellite

The signal flux density, i.e. the amount of electromagnetic power that passes through a given area in space per unit of frequency and typically expressed in W/m²/Hz (power over area over which the signal is spread, and over bandwidth where the signal is measured)[2], is one of the most important factors for a VLBI observations and it is used to characterize a VT signal. It depends on several factors such as properties of the VT, orbital configurations, atmospheric effects, and telescope specifications. The combined effects can be summarized by a link budget based on the gains and losses considering the transmitter power and other factors. A link budget for a VT can be written in dBW [3] with the following relationship:

Received Power [dBW] = Transmitted Power [dBW] + Gain [dBW] – Losses [dBW].

We have analyzed the received flux densities at VGOS telescopes observing the GENESIS satellite. The flux densities received at the ground stations from a VT onboard the GENESIS satellite are determined from the Power received ($\mathbf{P_r}$) calculating the transmitter power using the Friis transmission formula:

$$\frac{\mathbf{P_r}}{\mathbf{P_t}} = \frac{\mathbf{G_t G_r \lambda^2}}{(\mathbf{4\pi R})^2}$$

where P_r and P_t are the received and transmitted powers, G_t and G_r are the antenna and receiver gains, λ is the signal wavelength, and R is the distance between the VT and the ground station. For a standard flux density at the ground station of 1 Jy at the maximum distance, considering a bandwidth of 200 MHz, the required transmitter power is around -26 dBW at maximum distance (for an elevation angle corresponding to 5 degrees). The required transmitter power is computed by considering the free space path loss and telescope gains only We do not consider atmospheric attenuation effects in the analysis. We have used this value as the baseline transmitter power for the simulations considering an isotropic VT antenna. We have then evaluated the received spectral flux densities at 12 VGOS stations during a one-day observation of the GENESIS satellite, which is in a polar orbit at an altitude of 6000 km, assuming an isotropic antenna radiation with $G_t = 1$ (our results can be normalized with the actual gain of the antenna if necessary). The locations of the VGOS stations are the same as in the previous section. Our simulations consider all possible observations at five-minute intervals with an elevation threshold at 5 degrees.
Figure 11 shows the histogram (normalized to one) of received flux density differences across all possible baselines for each observation in the simulations. The histogram demonstrates that stations generally receive similar flux densities from an isotropic antenna, indicating consistency and reliability in the model. For example, almost 16% of all observations has a difference within 0 and 0.1 Jy for each baseline stations. To further elaborate this trend, Figure 12 plots the received flux densities for individual stations across all observations. The results are consistent with the initial assumption of a received flux density of 1 Jansky at the maximum distance. At maximum distances (corresponding to minimum elevations), the flux density is approximately 1 Jansky, whereas at minimum distances (or zenith observations), it increases to about 2.85 Jansky. These findings are in

[2] The standard unit of flux density is watts per square meter per hertz (W/m²/Hz), but in radio astronomy, it is often expressed in Janskys (Jy), where 1 Jy=10^{-26} W/m²/Hz.

[3] dBW is a unit of absolute power expressed in decibels relative to 1 Watt: $P_{\mathrm{dBW}} = 10\log_{10}\left(\frac{P_{\mathrm{Watt}}}{1\ \mathrm{Watt}}\right)$.

line with the histogram, where the maximum flux density difference is observed to be around 1.80 Jansky in the case of antenna isotropy assumption.

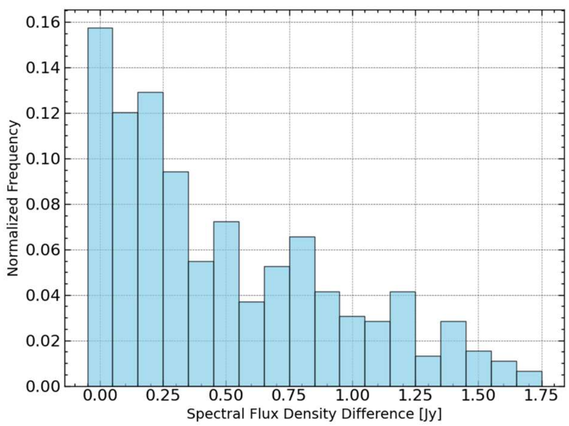

Figure 11. Normalized histogram (noted "Normalized frequency") of received flux density differences of the baseline stations for all possible observation. The differences are truncated to 0.1 Jy.

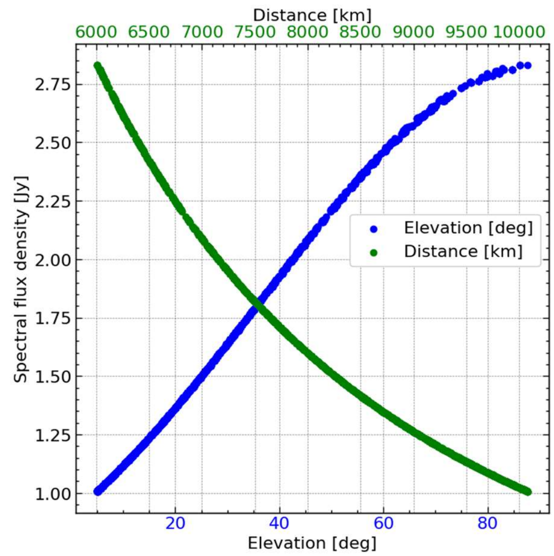

Figure 12. Received flux densities with respect to distances and elevations for all individual VGOS stations from an isotropic antenna with a transmit power of ~ -26 dBW and bandwidth of 200 MHz.

To further analyse the differences in received flux densities for individual baseline observations, Figure 13 illustrates the maximum differences between baselines during the simulation. The results indicate that relatively short baselines, such as KOKEE12M-ONSALA and GGAO12M-WESTFORD, exhibit similar flux density differences during the observation period. This behaviour can be attributed to the common visibility geometry of the ground stations: the elevation angles of the GENESIS satellite in the sky of both stations often align, resulting in similar distances to the satellite and, consequently, comparable flux densities. Similarly, long baselines, such as WESTFORD-ISHIOKA and RAEGYEB-ISHIOKA, also experience comparable flux density differences. The reason for that is also due to possible geometrical options. A satellite around Genesis altitude is only visible by distant baselines if both of them have similar small elevations. Otherwise, one of them cannot see the satellite and observation condition cannot be satisfied. Both stations having similar distances results in similar distances hence similar flux densities. Figure 14 further illustrates the relationship between baseline length and elevation angles. While shorter and longer baselines generally exhibit similar flux densities, mid-range baselines display greater variability. This variability occurs because, for mid-range baselines, one station may observe the satellite at a high elevation angle while the other observes it at a lower elevation angle. This difference in viewing geometry leads to a wider range of flux density differences for mid-length baselines.

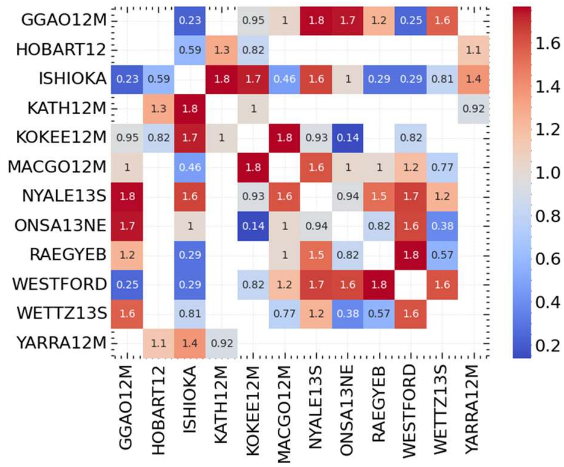

Figure 13. Maximum difference between the received flux densities for each baseline of VGOS network considering an isotropic antenna with a transmit power of -25.9 dBW and bandwidth of 200 MHz.

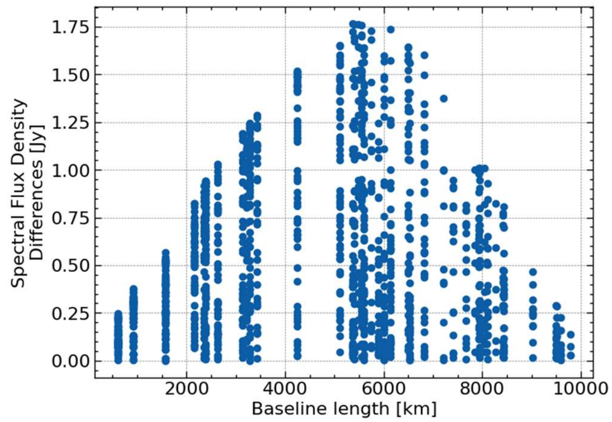

Figure 14: Maximum difference between the received flux densities with respect to baseline lengths considering an isotropic antenna with a transmit power of -25.9 dBW and bandwidth of 200 MHz.